Appl Compos Mater (2018) 25:309–320
DOI 10.1007/s10443-017-9622-8

Experimental Study and Numerical Modelling of Low Velocity Impact on Laminated Composite Reinforced with Thin Film Made of Carbon Nanotubes

A. El Moumen [1] · M. Tarfaoui [1] · O. Hassoon [1] · K. Lafdi [2] · H. Benyahia [1] · M. Nachtane [1]

Received: 14 June 2017 / Accepted: 28 June 2017 / Published online: 18 July 2017

Abstract In this work, polymer laminated composites based on Epon 862 Epoxy resin, T300 6 k carbon fibers and carbon nanotubes (CNTs) were tested with the aim to elucidate the effect of CNTs on impact properties including impact force and capacity to absorb impact energy. The polymer matrix was reinforced by a random distribution of CNTs with fraction ranging from 0.5 to 4.wt%. Composite panels were manufactured by using the infusion process. Taylor impact test was used to obtain the impact response of specimens. Projectile manufactured from a high strength and hardened steel with a diameter of 20 mm and 1.5 kg of mass was launched by a compressed gas gun within the velocity of 3 m/s. Impact force histories and absorbed energy of specimens were recorded. A numerical model was employed to simulate the impact performance. This model has been accomplished by forming a user established subroutine (VUMAT) and executing it in ABAQUS software. Finally, the effect of CNTs amount on dynamic properties of laminated composites was discussed.

Keywords Carbon nanotubes · Polymer composite materials · Low-velocity impact · Dynamic properties · Numerical modelling · Damage modelling · VUMAT

1 Introduction

The development of functional laminate polymer composites with specific electrical, thermal and mechanical properties is an important research area for the integration of sensing functionalities into composite materials. Carbon nanotubes (CNTs) can be implanted within a composite structures through integration with the matrix [1–3], fiber [4] or both [5].

✉ A. El Moumen
ahmed.el_moumen@ensta-bretagne.fr

[1] ENSTA Bretagne, CNRS FRE 3744, IRDL, F-29200 Brest, France

[2] University of Dayton Research Institute, Dayton, OH 45469-0168, USA

Implantation of CNTs within the matrix mainly addresses resin dominated properties such as impact resistance, transverse properties and delamination [6]. On the other hand, incorporating CNTs onto fiber reinforcement surface has the potential to improve fiber/matrix adhesion, mainly via a cross-link connection created with nanotubes.

Much interest has been directed to examining the impact strength of hybrid CNTs composites by means of drop test. For example, Soliman et al. [7, 8] introduce pristine and functionalized multi-wall CNTs by dispersing them into the epoxy matrix polymer and observed an improvement in the matrix-dominated properties such as interlaminar shear strength. The effect of the addition of 0.5 wt.% of CNTs on the impact properties of a Carbon fibers/polymer was studied by Kostopoulos et al. [9] and Benyahia et al. [10]. Experimental drop test was used by Soliman et al. [8] in order to determine the low-velocity impact response of thin carbon laminate composites reinforced with functionalized multi-walled carbon nanotubes. Three percentages of CNTs by weight of epoxy were considered as; 0.5%, 1.0%, and 1.5% and the composite plates were subjected to different levels of energy: 15, 24, 30, 60, and 120 J. the authors observed that the functionalized CNTs enhanced the impact response and limited the damage size in the laminate composite. Charpy test was employed by Laurenzi et al. [11] for composite materials reinforced with CNTs to determine the capability of absorbing energy during impact test. The tests were conducted at different weight percentages of CNT into epoxy resin. Results of the Charpy test showed that the presence of CNTs increases the toughness of the composite up to a threshold value of 0.5 wt.%. It should be mention that a few studies examined the use of CNTs film to improve the impact response of laminated composites. Hosur et al. [12] studied the impact response of woven carbon/epoxy but with nanoclay reinforcement and observed no change in the impact response.

Energy absorption capability and impact force are the main variables analyzed during impact testing. This article further examines the use of this film made of CNTs/epoxy to improve the low-velocity impact response of textile composites. Firstly, we have interested to the case of impact with damaged surface and without perforation of panels using Taylor gun. In this study, the use of a wide range of CNTs loadings, ranging from 0.5 to 4 wt.%, in epoxy composites is studied. The experimental results are compared to the case of neat composites. In addition, experimental test is accomplished by forming a numerical model with user established sub-routine VUMAT and executing it in ABAQUS software. A comparison between results of experience and numerical model is given.

2 Constitutive Progressive Degradation of Composite Material

Progressive failure models have been adopted in the finite element simulations to model the onset of damage and his propagation in composite materials based on the concept of the continuum damage mechanics (CDM). The material behavior can be characterized in two substantial phases namely the elastic and the failure regions. The elastic region means that the material can be come back to original shape dimensions without deformation when unloading. This phenomenon appears because the material have an elastic energy depended on material nature type. In the other hand, the second phase represents as post failure region, followed subsequent to the material satisfied the onset of the damage, and further loading results in a degradation of mechanical properties of the structure and subsequently to a reduction in its

stiffness caused by the accumulation of cracks. The relationship between the effective stress (σ) and nominal stress (σ) can be defined in form:

$$\hat{\sigma} = d.\sigma \tag{1}$$

Where d is the damage operator.

Thus stress with presence of the damages is given as:

$$\sigma_{i,j} = C_{i,j}\,(d).\varepsilon_{i,j} \tag{2}$$

where C represents the undamaged orthotropic stiffness matrix. This matrix takes the following form:

$$C = \begin{bmatrix} C_{11} & C_{12} & C_{13} & 0 & 0 & 0 \\ C_{12} & C_{22} & C_{23} & 0 & 0 & 0 \\ C_{13} & C_{23} & C_{33} & 0 & 0 & 0 \\ 0 & 0 & 0 & C_{44} & 0 & 0 \\ 0 & 0 & 0 & 0 & C_{55} & 0 \\ 0 & 0 & 0 & 0 & 0 & C_{66} \end{bmatrix} \tag{3}$$

Then the damage stiffness matrix is as follow [13]:

$$\begin{aligned} dC_{11} &= (1-d_f)\ E_1\left(1-v_{23}^2\right)\ \Gamma\ , & dC_{22} &= (1-d_f)\ (1-d_m)\ E_2\left(1-v_{13}^2\right)\ \Gamma \\ dC_{33} &= (1-d_f)\ (1-d_m)\ E_3\left(1-v_{21}^2\right)\ \Gamma\ , & dC_{12} &= (1-d_f)\ (1-d_m)\ E_1(v_{21}-v_{31}v_{23})\ \Gamma \\ dC_{23} &= (1-d_f)\ (1-d_m)\ E_2(v_{32}-v_{12}v_{31})\ \Gamma\ , & dC_{31} &= (1-d_f)\ (1-d_m)\ E_1(v_{31}-v_{21}v_{32})\ \Gamma \\ dC_{44} &= (1-d_f)(1-d_{mt}s_{mt})E_1(1-d_{mc}s_{mc})G_{12}, & dC_{55} &= (1-d_f)(1-d_{mt}s_{mt})E_1(1-d_{mc}s_{mc})G_{23} \\ dC_{66} &= (1-d_f)(1-d_{mt}s_{mt})E_1(1-d_{mc}s_{mc})G_{31}, \end{aligned} \tag{4}$$

where the damage variables and Γ are given by Eq. 5 [13]:

$$\begin{aligned} d_f &= 1 - \left(1-d_{ft}\right)\ \left(1-d_{fc}\right) \\ d_m &= 1 - \left(1-d_{mt}\right)\ \left(1-d_{mc}\right) \\ \Gamma &= 1/\left(1-v_{12}^2-v_{23}^2-v_{13}^2-2\,v_{12}v_{23}v_{13}\right) \end{aligned} \tag{5}$$

Where d_f, d_m and d_s is the damage variables for the fiber, matrix and shear failure mode respectively.

2.1 Intralaminar Failure Criteria

The damage initiation occurs when the true applied stress in the laminate composite reaches the ultimate strength of the ply laminate. Explicitly, damage occurs to the interface due to a difference between the transverse compressive fibre modulus and the matrix modulus, which represents the main cause of damage initiation. A user material VUMAT subroutine was coded in FORTRAN language and executed by the finite element explicit Abaqus software to characterise the intralaminar damage. The failure onset was based on Hashin failure criteria in three dimensional form for fibres and matrices. These criteria have been widely applied to predict the initiation of damage in unidirectional composites [14, 15]. In the present study, these criteria were proposed for both fibers and matrix, and listed in Table 1.

Table 1 Hashin failure criteria [14]

Fiber Tensile Failure ($\sigma_{11} \geq 0$)	$f_{ft} = \left(\frac{\sigma_{11}}{X_t}\right)^2 \geq 1$
Fiber Compression Failure ($\sigma_{11} < 0$)	$f_{fc} = \left(\frac{\sigma_{11}}{X_c}\right)^2 \geq 1$
Matrix Tensile Failure ($\sigma_{22} + \sigma_{33}) \geq 0$	$f_{mt} = \frac{(\sigma_{22}+\sigma_{33})^2}{{Y_t}^2} + \frac{{\sigma_{23}}^2 - \sigma_{22}\sigma_{33}}{S_{23}^2} + \left(\frac{\sigma_{12}}{S_{12}}\right)^2 + \left(\frac{\sigma_{13}}{S_{13}}\right)^2 \geq 1$
Matrix Compression Failure ($\sigma_{22} + \sigma_{33}) < 0$	$f_{mc} = \frac{1}{Y_c}\left(\left(\frac{Y_c}{2S_{23}}\right)^2 - 1\right)(\sigma_{22} + \sigma_{33}) + \frac{(\sigma_{22}+\sigma_{33})^2}{4{S_{23}}^2} + \frac{{\sigma_{23}}^2 - \sigma_{22}\sigma_{33}}{S_{23}^2} + \left(\frac{\sigma_{12}}{S_{12}}\right)^2 + \left(\frac{\sigma_{13}}{S_{13}}\right)^2 \geq 1$

2.2 Damage Evolution

As previously stated, after the initial failure criteria have been satisfied, further loading leads to regression of material stiffness, therefore, the properties of the material point were modified according to a material property degradation model. Based on the relationship between the effective stress and displacement, damage evolution can be constituted. Therefore, damage variables for each mode in the fibres and matrices are expressed in the form of the displacement:

$$d_i = \frac{\delta^f_{i,eq}\left(\delta_{i,eq} - \delta^0_{i,eq}\right)}{\delta_{i,eq}\left(\delta^f_{i,eq} - \delta^0_{i,eq}\right)} \quad , \quad \delta^0_{i,eq} \leq \delta_{i,eq} \leq \delta^f_{i,eq} \tag{6}$$

Where d_i is the damage variable defined for each damage mode. The variables δ^0_{eq}, δ_{eq} and $\delta^f_{i,eq}$ represent respectively the initial displacement when the failure criterion is reached, the equivalent displacement and the equivalent failure displacement. These displacements can be computed from the fracture energy corresponding to each damage variable as follow:

$$\begin{aligned} G_i = \int_{\delta^0_{i,eq}}^{\delta^f_{i,eq}} \sigma \, d\varepsilon &= \frac{1}{2}\left(\delta^f_{i,eq} - \delta^0_{i,eq}\right)\sigma^0_{i,eq} \\ \delta^f_{i,eq} - \delta^0_{i,eq} &= \frac{2G_i}{\sigma^0_{i,eq}} \\ \delta^0_{i,eq} &= \delta_{i,eq}/\sqrt{f_i} \\ \sigma^0_{i,eq} &= \sigma_{i,eq}/\sqrt{f_i} \end{aligned} \tag{7}$$

$\sigma_{i,eq}$, $\sigma^0_{i,eq,}$, f_i and G_i are respectively equivalent stress, equivalent initial stress, initial failure and the fracture energy corresponding to each mode. These variables are computed for each element's integration point to describe the material's stiffness degradation for every damage mode as described in Table 2. The equivalent displacement and equivalent stress are determined for each iteration until the complete failure ($d_f = 1$) of element occurs. At this point, the element deletes from the model and its stresses become zero. Thus, the stiffness of the element is removed from the laminate stiffness [16].

Where $\langle \varepsilon_{ii} \rangle$ is the Macaulay operator and calculated as:

$$\langle \varepsilon_{ii} \rangle = \frac{\varepsilon_{ii} + |\varepsilon_{ii}|}{2} \tag{8}$$

L_c is characteristic length, which is defined to overcome the strain localisation when the material exhibits strain-softening behaviour [17], and thus is integrated into the model to

Table 2 Equivalent displacement and equivalent stress for each mode [16]

Failure mode	$\delta_{i,eq}$	$\sigma_{i,eq}$
Fibre tensile damage mode	$L_c\sqrt{(\varepsilon_{11})^2+(\varepsilon_{12})^2+(\varepsilon_{31})^2}$	$L_c(\sigma_{11}\varepsilon_{11}+\sigma_{12}\varepsilon_{12}+\sigma_{31}\varepsilon_{31})/\delta_{1,eq}$
Fibre compressive damage mode	$L_c\sqrt{\left(-\varepsilon_{11}-\frac{\langle\varepsilon_{33}\rangle.\,E_{33}}{E_{11}}\right)^2}$	$L_c\left(E_{11}\left(-\varepsilon_{11}-\frac{\langle\varepsilon_{33}\rangle.\,E_{33}}{E_{11}}\right)\right)/\delta_{2,eq}$
Matrix tensile damage mode	$L_c\sqrt{(\varepsilon_{22})^2+(\varepsilon_{12})^2+(\varepsilon_{23})^2}$	$L_c(\sigma_{22}\varepsilon_{22}+\sigma_{12}\varepsilon_{12}+\sigma_{23}\varepsilon_{23})/\delta_{3,eq}$
Matrix compressive damage mode	$L_c\sqrt{\left(-\varepsilon_{22}-\frac{\langle\varepsilon_{33}\rangle.\,E_{33}}{E_{22}}\right)^2+(\varepsilon_{12})^2}$	$L_c\left(E_{22}\left(-\varepsilon_{22}-\frac{\langle\varepsilon_{33}\rangle.\,E_{33}}{E_{22}}+\sigma_{12}\varepsilon_{12}\right)\right)/\delta_{2,eq}$

render the absorbed energy independent of the mesh sensitivity. In the solid element case, the characteristic length is obtained by the cube root of the area associated with the material point.

3 Materials, Properties and Manufacturing Process

3.1 Materials

The polymer used in this study is Epon 862 Epoxy resin, which is suited for resin infusion techniques due to a low viscosity. T300 6 k carbon fibers fabric provided by Hexell was used. Multiwall CNTs purchased from Nanocyl, Belgium, are used as reinforcement and to prepare a thin layer nanocomposite films. The average diameters of nanotubes were of the order of 10 nm, 1.5 μm of length, purity >95% and transition metal oxide <1%. Multiwall CNTs are produced via the Catalytic Chemical Vapor Deposition process.

3.2 Machined Panels

For the fabrication of composite panels, two steps were performed: (1) fabrication of nanocomposite film made of epoxy resin reinforced with CNTs randomly distributed and (2) placement of this nanocomposite film between plies of laminates. Manufacturing process was presented in our previous work [2, 3, 18] and illustrated in Fig. 1.

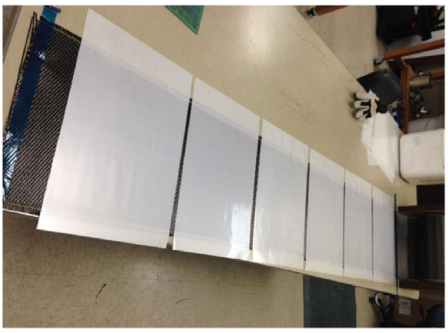

(a) Nanocomposite film placed on the carbon fabric

(b) Stacks of carbon Fabric with Nanocomposite film as interleave

Fig. 1 Placement of nanocomposite film onto woven fabrics

Manufacturing process is conducted at University of Dayton, Ohio. First, fraction of nanotubes were mixed with Epoxy resin using a high shear laboratory mixer at 2000 rpm for 30 min, and then the ultrasonic path was used to obtain a homogeneous mixture and to guarantee a better random distribution of CNTs. Then we take the mixture in three rolls paint mill. The fraction of nanotubes was varied between 0.5% and 4% based on the final needed. The film with 120 μm in thickness containing CNTs randomly oriented is manufactured using film line, Fig. 2a. Once the film is prepared, we make composite panels with the film as interleave between carbon fiber fabrics and cured in hot press. All composite panels were fabricated with 5-Harness satin weave fabric using infusion process. Each panel consisted of 12 layers of carbon fiber fabric interleaved with 12 layers of epoxy/CNTs nanocomposites film with a target fiber volume of 50%. Panels were press cured according to manufacturer's cure cycle under a pressure of 200 MPa. After the panels had cooled, they were prepared for mechanical testing. Final thickness of panels is nominally 4 mm.

3.3 Mechanical Properties of Composites

The mechanical properties of the composite panels used in this study were determined in our previous work using static experimental test. These properties are listed in Table 3.

4 Methodology of Characterization

4.1 Experimental Setup

For the impact test, Taylor gun was used to perform these tests at the ENSTA Bretagne, France. It is equipped with a 5 l tank capacity, filled with compressed air and a valve for the electro-pneumatic control valve. The velocity of the projectile striking the target was measured by a pair of photodiodes as the projectile passed through the light beams. The impact speed typically reaches up to 120 m/s. The samples are simply held on the support mounted on the load cell.

The force is measured by a 50 × 200 mm cylindrical calibrated cell attached to the barrel stop. Equipped with strain gauges, it works according to the principle of the Wheatstone bridge

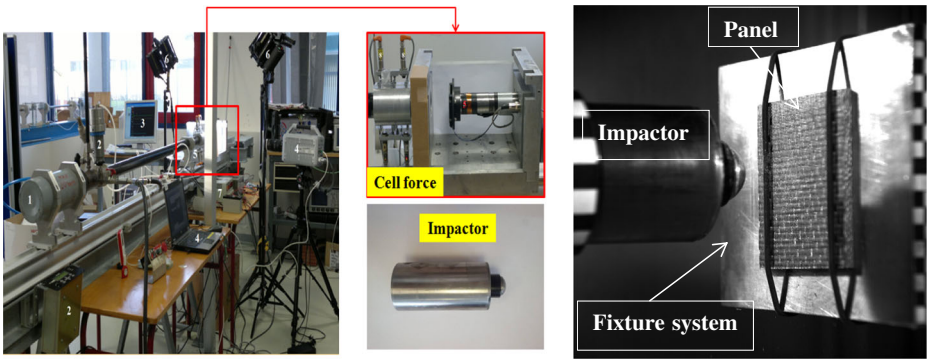

Fig. 2 Experimental test: Taylor gun assembly, impactor, cell force and the composite panel

Table 3 Orthotropic elastic properties of composite panels

	0%	0.5%	1%	2%	4%
(a) Predicted Young's moduli versus percentage of CNTs					
E_{11} (GPa)	59.11	59.138	59.16	59.219	59.33
E_{22} (GPa)	59	59	59	59	58.55
E_{33} (GPa)	7.6	7.623	7.6	7.67	7.81
(b) Predicted Poisson ratio versus percentage of CNTs					
ν_{12}	0.089	0.089	0.0892	0.0892	0.0892
ν_{13}	0.27	0.27	0.27	0.274	0.275
ν_{23}	0.28	0.28	0.277	0.279	0.28
(c) Predicted shear moduli versus percentage of CNTs					
G_{12} (GPa)	8.25	8.257	8.27	8.285	8.316
G_{23} (GPa)	3.97	3.99	4.017	4.04	4.105
G_{13} (GPa)	0.27	0.27	0.27	0.274	0.275

for the measurement of the deformation during the test. A hardened steel impact of 50 mm diameter and a 20 mm hemispherical head was used with 1.6 kg of mass. Figure 2 shows the Taylor gun used for tests, panels and fixture system and the impactor form.

4.2 Numerical Procedure

Numerical model of impact test was created with help of Abaqus software in accordance with the experimental conditions such as the panel geometry, the fixture system, and the impactor shape and size as shown in Fig. 3. Abaqus was chosen for the low velocity impact analysis of laminate structures as it is general-purpose software for analysis of large deformation and dynamic response of composite based on explicit time integration. The cell force was modelled as rigid materials to replicate the boundary conditions of the experiment. The square composite panels of 12 plies and 70 × 70 × 4 mm^3 of dimensions were modelled with 8-nodes linear brick of type element and reduced integration C3D8R. The

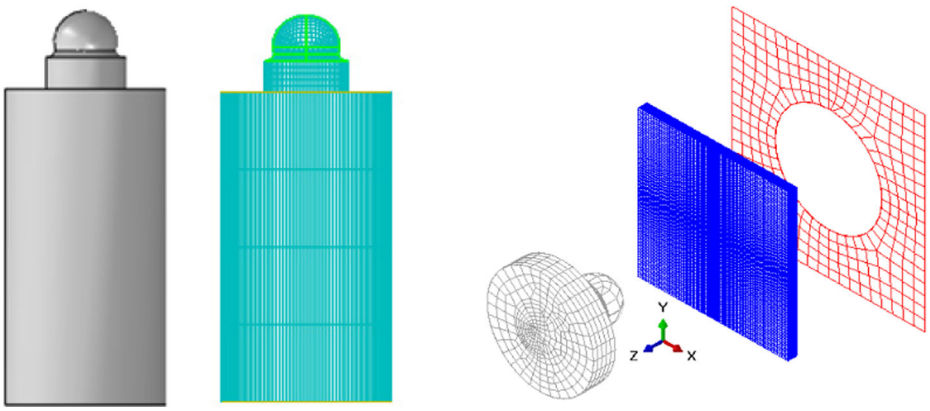

(a) Impactor (b) Full model

Fig. 3 Numerical model for impact test: impactor, composite panels and cell force

hemispherical impactor is modelled with 14,136 solid elements. The impact velocity that was measured during the experiments was defined to the nodes of the impactor. The penalty contact method is considered in order to represent the contact between the projectile and the laminate plate with frictionless.

In the local impact region, the mesh was refined which was progressively coarser toward the external plate edges, with one thick element for each layer [19–21]. In all plates with different weight of the percentage of carbon nanotubes, a low velocity impact was performed with 3 m/s, which corresponding to kinetic energy of 7.2 J.

5 Results and Discussion

5.1 Force-Time History

For experimental characterization, each test was repeated three times in order to ensure the reproducibility of curves. The force variation of every test was plotted to analyse the dynamic response of the specimens. Example of curves obtained experimentally and compared with numerical results is shown in Fig. 4 for different % of CNTs. It can be seen that the impact force histories of all composite panels show the same tendency for different percentage of CNTs. No more difference is observed between numerical results and experimental data. The force curve exhibiting an almost linear increase as the projectile contacts the panel. A sudden drop in the force-time history curves is observed after it reaches the first peak value, which indicates a loss of stiffness caused by damage initiation in the contact surface (especially matrix cracking). It should be mentioned that there is oscillation existing in the curves of forces which is caused by damage of panels [18, 22] or the elastic wave propagation in the panel and projectile [23]. These oscillations are also observed in curves of numerical model. Experimental results indicate that the peak force of composite panels with CNTs is the highest compared with neat panels, Fig. 5. The peak force and test duration for impact simulation are comparable to the experimental impact test. It could be seen that a small difference is obtained after peak force between the two curves. Also, it can be noted that the slopes of the initial part of the force-time curves of the different panels are similar for the experiment and simulation. The sudden drop in the force value observed in the simulation corresponds to the penetration of impactor into the top facesheet, Fig. 6.

5.2 Energy Absorption Capacity of Carbon Nanotubes under Impact Test

The absorbed energy is the energy absorbed by structures through the formation of damage and the friction between the impacted specimens and the impactor. The internal energy-time responses for various loadings of nanotubes are shown in Fig. 7. It is concluded that the energy absorption capability of the specimens containing CNTs becomes important and increased compared to the case of 0%-CNTs. For example 3 J of absorbed energy is observed in the case of composite panels with 4%-CNTs, while specimens with 0%-CNTs provide approximately 4 J. Given that the energy absorption capacity is typically an indication of damage size in the composite, the addition of CNTs reduced composite damage significantly. Composites with 0%-CNTs absorb much energy by forming damage, while 4%-CNTs reduce the damage

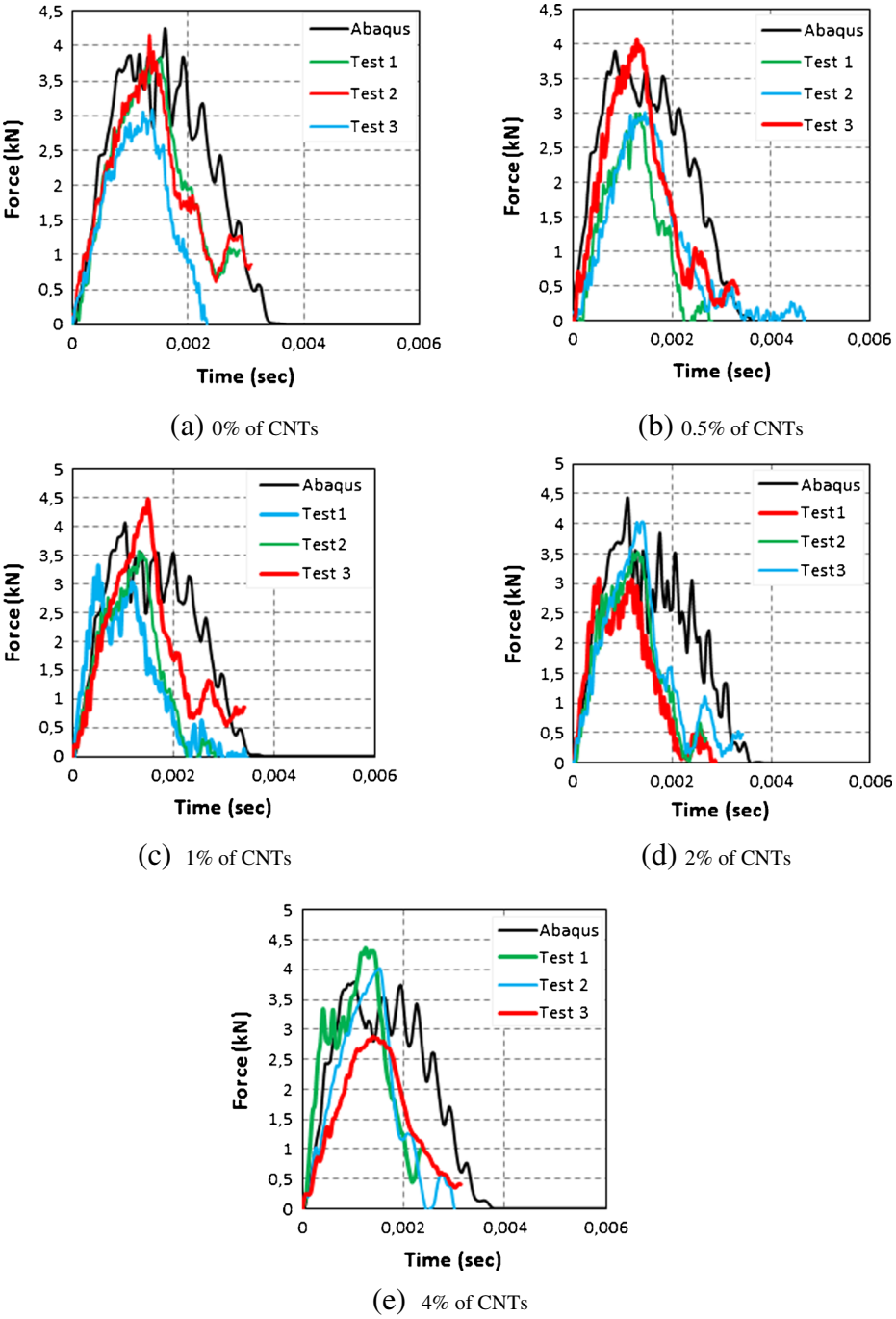

(a) 0% of CNTs

(b) 0.5% of CNTs

(c) 1% of CNTs

(d) 2% of CNTs

(e) 4% of CNTs

Fig. 4 Force-time curves vs CNTs loading, V = 3 m/s

size by absorbing the shock wave. Thus, the presence of CNTs absorbs a fraction of the energy.

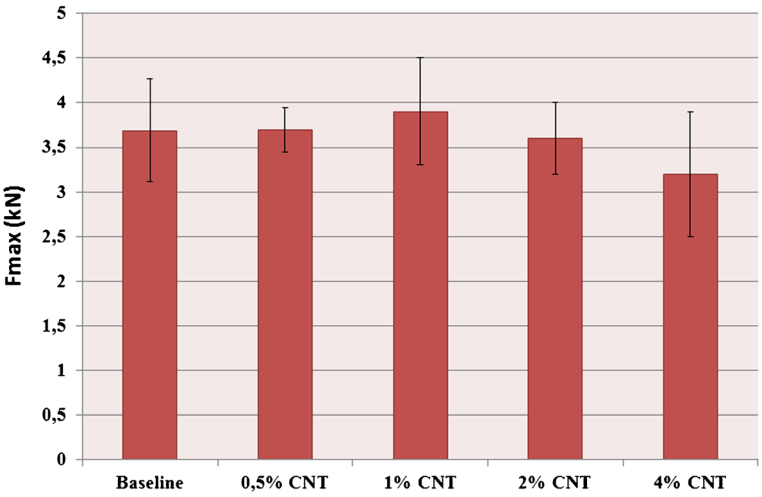

Fig. 5 Variation of force vs CNT fraction for experimental test

6 Conclusion

Experimental investigation and numerical modelling of low velocity impact test on laminate carbon fabric composites reinforced with various loadings of carbon nanotubes (CNTs) 0%, 0.5%,1.0%, 2% and 4% by wt. of epoxy are conducted. The composite plates were subjected

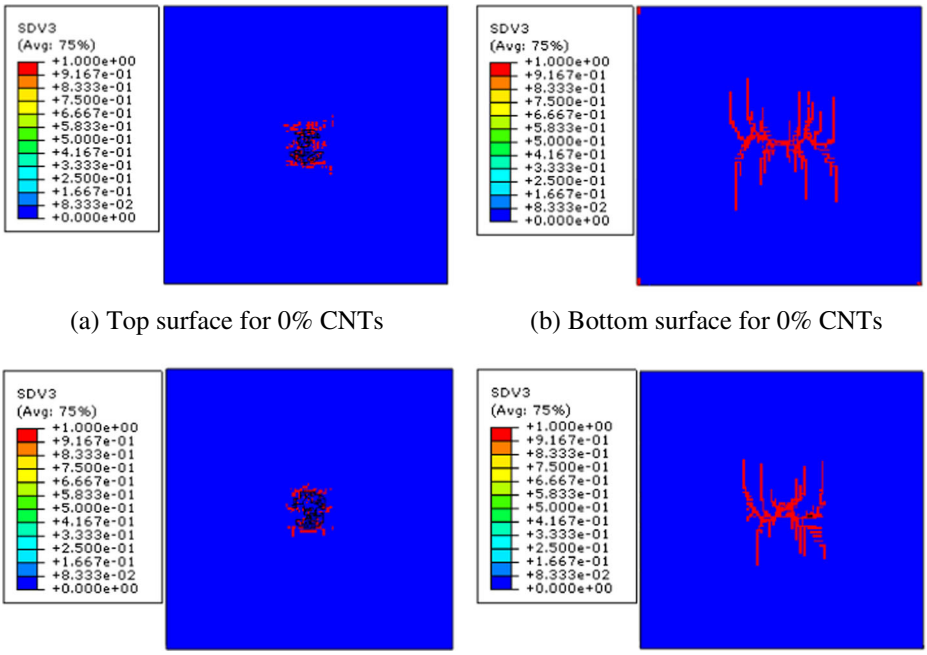

(a) Top surface for 0% CNTs (b) Bottom surface for 0% CNTs

(c) Top surface for 0.5% CNTs (d) Bottom surface for 0.5% CNTs

Fig. 6 Damaged zone predicted by the numerical model, V = 3 m/s

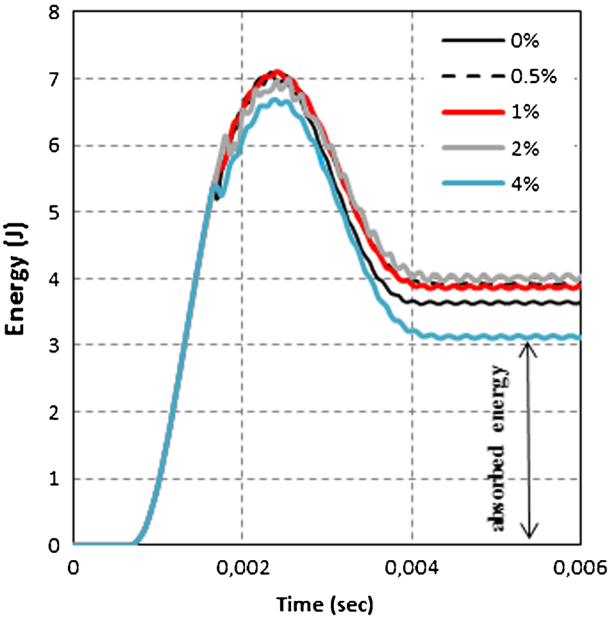

Fig. 7 Energy-time response versus percentage of CNTs, V = 3 m/s

to 3 m/s of impact velocity. Force-time curves and the absorbed energy history are determined and analyzed for different CNTs loading. Experimental results show that the maximum peak force is observed in the case of composites with CNTs compared to the case of neat panels. It show also that the energy absorption capability of the specimens containing CNTs becomes important and increased compared to the case of 0%-CNTs. Therefore, the addition of CNTs reduced composite damage significantly. Numerical model has been accomplished by forming a user established sub-routine (VUMAT) and executing it in ABAQUS software. The comparison shows that the numerical model gives the good results confronted with the experimental curves.

Acknowledgements This work was partially funded by DGA (Direction générale de l'armement - Ministry of Defense), MRIS project. The Authors of this paper gratefully acknowledge the financial support of the DGA, France. Acknowledgments have also addressed to Pr. Bruno Mortaigne at DGA-DS-MRIS, RDS Matériaux Chimie Energie departement.

References

1. Gojny, F.H., Wichmann, M.H.G., Fiedler, B., Bauhofer, W., Schulte, K.: Influence of nano-modification on the mechanical and electrical properties of conventional fiber-reinforced composites. Compos. A-Appl. Sci. **36**, 1525–1535 (2005)
2. Tarfaoui, M., Lafdi, K., El Moumen, A.: Mechanical properties of carbon nanotubes based polymer composites. Compos. Part B. **103**, 113–121 (2016)
3. El Moumen, A., Tarfaoui, M., Lafdi, K.: Mechanical characterization of carbon nanotubes based polymer composites using indentation tests. Compos. Part B. **114**, 1–7 (2017)
4. Garcia, E.J., Wardle, B.L., Hart, A.J., Yamamoto, N.: Fabrication and multifunctional properties of a hybrid laminate with aligned carbon nanotubes grown in situ. Compos. Sci. Technol. **68**, 2034–2041 (2008)

5. Warrier, A., Godara, A., Rochez, O., Mezzo, L., Luizi, F., Gorbatikh, L., et al.: The effect of adding carbon nanotubes to glass/epoxy composites in the fiber sizing and/or the matrix. Compos. A-Appl. Sci. **41**, 532–538 (2010)
6. Ashrafi, B., Guan, J., Mirjalili, V., Zhang, Y., Chun, L., Hubert, P., Simard, B., Kingston, C.T., Bourne, O., Johnston, A.: Enhancement of mechanical performance of epoxy/carbon fiber laminate composites using single-walled carbon nanotubes. Compos. Sci. Technol. **71**, 1569–1578 (2011)
7. Soliman, E., Al-Haik, M., Taha, M.R.: On and off-axis tension behavior of fiber reinforced polymer composites incorporating multi-walled carbon nanotubes. J. Compos. Mater. **46**, 1661–1675 (2011)
8. Soliman, E.M., Sheyka, M.P., Taha, M.R.: Low-velocity impact of thin woven carbon fabric composites incorporating multi-walled carbon nanotubes. Int. J. Impact Eng. **47**, 39–47 (2012)
9. Kostopoulos, V., Baltopoulos, A., Karapappas, P., Vavouliotis, A., Paipetis, A.: Impact and after-impact properties of carbon fibre reinforced composites enhanced with multi-wall carbon nanotubes. Compos. Sci. Technol. **70**, 553–563 (2010)
10. Benyahia, H., Tarfaoui, M., Datsyuk, V., El Moumen, A., Trotsenko, S., Reich, S.: Dynamic properties of hybrid composite structures based multiwalled carbon nanotubes. Compos. Sci. Technol. **148**, 70–79 (2017)
11. Laurenzi, S., Pastore, R., Giannini, G., Marchetti, M.: Experimental study of impact resistance in multi-walled carbon nanotube reinforced epoxy. Compos. Struct. **99**, 62–68 (2013)
12. Hosur, M.V., Chowdhury, F., Jeelani, S.: Low-velocity impact response and ultrasonic NDE of woven carbon/epoxy–nanoclay nanocomposites. J. Compos. Mater. **41**, 2195–2212 (2007)
13. Guo, W., Xue, P., Yang, Y.: Nonlinear progressive damage model for composite laminates used for low-velocity impact. Appl. Math. Mech. **34**, 1145–1154 (2013)
14. Hashin, Z.: Failure criteria for undirectional fiber composites. J. Appl. Mech. **31**, 223–232 (1980)
15. Wang, S., Wu, L., Ma, L.: Low-velocity impact and residual tensile strength analysis to carbon fiber composite laminates. Mater. Des. **31**, 118–125 (2010)
16. Xin, S.H., Wen, H.M.: A progressive damage model for fiber reinforced plastic composites subjected to impact loading. Int. J. Impact Eng. **75**, 40–52 (2015)
17. Lapczyk, I., Hurtado, J.A.: Progressive damage modeling in fiber-reinforced materials. Compos. A: Appl. Sci. Manuf. **38**, 2333–2341 (2007)
18. El Moumen, A., Tarfaoui, M., Lafdi, K., Benyahia, H.: Dynamic properties of carbon nanotubes reinforced carbon fibers/epoxy textile composites under low velocity impact. Compos. Part B. **125**, 1–8 (2017)
19. Hassoon, O.H., Tarfaoui, M., El Moumen, A.: Progressive damage modeling in laminate composites under slamming impact water for naval applications. Compos. Struct. **167**, 178–190 (2017)
20. Nachtane, M., Tarfaoui, M., El Moumen, A., Saifaoui, D.: Damage prediction of horizontal axis marine current turbines under hydrodynamic, hydrostatic and impacts loads. Compos. Struct. **170**, 146–157 (2017)
21. Tarfaoui, M., El Moumen, A., Lafdi, K.: Progressive damage modeling in carbon fibers/carbon nanotubes reinforced polymer composites. Compos. Part B. **112**, 185–195 (2016)
22. Ren, Y., Jiang, H., Ji, W., Zhang, H., Xiang, J., Yuan, F.G.: Improvement of progressive damage model to predicting crashworthy composite corrugated plate. Appl. Compos. Mater. (2017). doi:10.1007/s10443-017-9610-z
23. Wang, H., Ramakrishnan, K.R., Shankar, K.: Experimental study of the medium velocity impact response of sandwich panels with different cores. Mater. Des. **99**, 68–82 (2016)